ARTICLES

Melting of Pb nanocrystals

Kevin F. Peters, Jerome B. Cohen, and Yip-Wah Chung

Department of Materials Science and Engineering, Robert R. McCormick School of Engineering and Applied Science,

Northwestern University, Evanston, Illinois 60208

The size-dependent melting and surface melting of Pb nanocrystals is demonstrated by x-ray powder diffraction in ultrahigh vacuum. Whereas some prior studies have measured the size-dependent melting temperature via the diffraction intensity, it is shown here that crystallite reorientation makes the diffraction intensity an unreliable indicator of melting. Instead of the diffraction intensity, the diffraction peak shape reveals the size-dependent melting via changes in the crystallite size distribution. Measurements showed that the melting temperature varies inversely with the crystallite size and quantitatively favors the liquid-skin melting model over the homogeneous melting model. Surface melting is demonstrated via the reversible growth of a 0.5 nm liquid skin on 50 nm crystallites just below the size-dependent melting temperature. [S0163-1829(98)04821-8]

I. INTRODUCTION

The important role of the surface in the melting process has long been suspected[1–8] and has recently been confirmed[9] via surface-sensitive measurements of melting. These recent measurements include structural demonstrations of liquid-skin formation on flat surfaces below the melting temperature of the interior crystal;[10–12] the dramatic melting temperature reduction of nanometer-sized particles in proportion to the surface-to-volume ratio;[13–24] and more recently, liquid-skin formation on the highly curved surfaces of nanocrystals below the size-dependent melting temperature.[25] Using techniques based on x-ray diffraction, the present study explores the ''bulk'' and surface melting of Pb nanocrystals, including a comparison between nanoparticle- and flat-surface melting.

The study of small-particle melting phenomena benefits from an understanding of flat-surface melting. The driving force for flat-surface melting is thought to be a reduction in the total interfacial energy, $\Delta\gamma < 0$, where[3,5,10–12,26]

$$\Delta\gamma = \gamma_{\ell v} + \gamma_{s\ell} - \gamma_{sv}. \tag{1}$$

γ is the interfacial energy per unit area, and s, ℓ, and v identify the solid, liquid, and vapor phases, respectively. It is known for Pb that the solid-vapor interfacial energy γ_{sv} varies by $\pm 3\%$ for different surface orientations.[27] Moreover, Pluis *et al.* and others have shown that some flat surface orientations of Pb exhibit flat-surface melting (i.e., $\Delta\gamma < 0$), while others do not ($\Delta\gamma > 0$).[10–12,26] Thus, for Pb and most cubic metals,[28] the ''average'' driving force for surface melting is close to zero (i.e., $\Delta\gamma \approx 0$), and subtle changes of surface conditions can have marked effects on surface melting.

Recent theories of small-particle surface melting[29–33] (which assume that $\Delta\gamma$ is isotropic and negative) predict that the liquid-skin thickness differs from that for a flat surface because of geometrical and capillary effects. For instance,

Baker and Dash[29] predict that the liquid-skin thickness on a nanocrystal might increase over the value for a flat surface in order to reduce the solid-liquid interfacial area and hence, the total interfacial energy. Geometrically, the liquid-skin thickness cannot exceed the particle radius, whereas the liquid-skin thickness diverges on most flat surfaces at the melting temperature of a semi-infinite solid.[3,10,12] Also, surface melting might be suppressed because the crystallite shape favors surface orientations with the lowest energy (γ_{sv}),[34] which are less prone to surface melting [Eq. (1)]. Since the driving force for surface melting is so small ($\Delta\gamma \approx 0$), one cannot know *a priori* if other factors, such as interactions between surface steps, might enhance liquid-skin growth on small particles or suppress it entirely.

Classically, the melting of small particles has been described by three models:

(1) Homogeneous melting model,[6,14,15] without a liquid skin,

(2) Liquid-skin melting model,[7,22,35] and

(3) Liquid nucleation and growth model,[8,21,33,36] with an unstable liquid skin.

Thus, a particle can be either a liquid droplet or a crystallite, which may have a uniform liquid skin that reduces the crystallite size. Thermodynamically, all three models predict a size-dependent melting temperature $T_m(D)$ that varies inversely with the crystallite diameter D as follows:

$$T_m(D) = 1 - 4\alpha/(\rho_s H D), \quad \text{for } 0 < T \leq 1, \tag{2}$$

where T is the reduced temperature [normalized to unity at the bulk melting temperature $T_m(\infty)$], ρ_s is the density of the solid, and H is the latent heat of fusion. The value of α can be shown to differ only slightly among the models, ignoring the solid-liquid density difference. For the homogeneous melting model, $\alpha_1 \approx (\gamma_{sv} - \gamma_{\ell v})$; and for the liquid-skin melting model, $\alpha_2 \approx \gamma_{s\ell}$. In model 3, α_3 can vary between a low-temperature limit of $1.5(\gamma_{sv} - \gamma_{\ell v})$ and an upper limit of $\gamma_{s\ell}$, so that the melting transition is ''smeared out.''[8] Al-

though prior investigators have tried to distinguish between the models using data on the size-dependent melting temperature, we note here that $(\alpha_2 - \alpha_1) = \Delta\gamma$ [see Eq. (1)]. Since $\Delta\gamma \approx 0$, the three models predict essentially the same size-dependent melting temperature.

The study by Buffat and Borel[14,15] inspired the present investigation. It included a critical review of the ''observational methods'' that had been used to measure the size-dependent melting temperature through 1975. $T_m(D)$ has now been measured by various methods for Pb,[13,16,19–21,23,24,37] Sn, Bi, In, Au, Ag, Cu, Ge, Al, Na, and CdS, including some more recent studies.[16,21,24,38–41] Overall, these studies of $T_m(D)$ agree with *all* the melting models. Buffat and Borel determined $T_m(D)$ of gold nanoparticles as a function of D down to 2.5 nm from a knowledge of the Au particle size distribution and the temperature variation of the Au 220 electron diffraction intensity up to $T_m(\infty)$. Allen *et al.*[16] measured $T_m(D)$ of individual nanocrystals of Pb, Sn, Bi, and In based on the disappearance of the electron-diffraction intensity. Using new techniques, Lai *et al.*[39] measured $T_m(D)$ by calorimetry, and Castro *et al.*[38] used the field-emission current from individual Au particles down to 2 nm to measure shape changes associated with melting in ultrahigh vacuum.

Despite the large body of data, the melting mechanism has remained unresolved because (1) most studies did not account for the effects of contamination, and (2) spurious effects may introduce ambiguity in the various observational methods, as outlined elsewhere.[14] For instance, the spurious influence of an electron beam on the nanoparticles has been widely reported.[16,23,34,37,42,43] In addition, we will show that crystallite reorientation makes the diffraction intensity an unreliable indicator of melting. Therefore, the numerous prior results that were obtained by electron-beam techniques or by the diffraction intensity from powders or single crystallites will not be commented upon further.

The present study employs x-ray techniques to provide measurements of the size-dependent melting together with the surface melting of Pb nanocrystals. We determine the total diffracting volume, average size, and size distribution of the crystallites via the diffraction peak intensity and shape.[44,45] These measurements are relatively immune to spurious effects, e.g., roughening or particle reorientation, which may have impaired previous analyses. When conducted under ultrahigh vacuum without electron beams, these experiments should be unaffected by contamination and electron-particle interactions.

II. EXPERIMENTAL METHOD

Sample preparation and x-ray-diffraction measurements were performed *in situ* in an ultrahigh vacuum chamber which had an x-ray transparent beryllium window.[46,47] The sample consisted of Pb particles supported on the native oxide surface of a Si (532)-oriented substrate. (With this orientation, the substrate scattered x rays very weakly.) Lead was chosen for several reasons, including its x-ray scattering strength, surface energy isotropy,[27] and well-characterized flat-surface melting.[10,11,26] Also, Pb is relatively inert. For example, at the surface of Pb, the sticking coefficient of gaseous H_2, H_2O, and O_2 is less than 0.005.[48–50] In the bulk, the

solid solubility of likely impurities (Si, O, C, H, or N) is very small so that the bulk melting temperature is reduced by only 1 K at saturation.[51,52] At the particle-substrate interface, Pb does not reduce silica nor wet it. In addition, the vapor pressure of Pb is low at the bulk melting temperature (3 $\times 10^{-9}$ Torr at 600 K).[53]

Samples were prepared *in situ* by evaporating Pb (Johnson Matthey, 99.9999%) from a resistively heated Ta boat onto the substrate. The substrate and Pb source were outgassed prior to deposition. The base pressure in the ultrahigh vacuum chamber was 3×10^{-9} Torr. The sample temperature was measured to within 0.1 K by a thermocouple in contact with the front side of the substrate but outside the x-ray beam. The temperature could be controlled to better than 0.5 K. The substrate was near room temperature during film deposition. The average film thickness was 2 to 5 nm. Immediately after deposition, samples were melted entirely and re-solidified. After sample preparation was complete, the sample was raised into position for x-ray-diffraction measurements.

X-ray diffraction scans were taken at various temperatures up to 600 K. An 18 kW rotating anode Cu x-ray source was used with an elastically bent, incident-beam LiF focusing monochromator set to pass only Cu $K\alpha_1$ radiation. The substrate surface normal was aligned for symmetric diffraction of the Pb 111 peak. A position-sensitive detector measured the scattered x rays simultaneously over an angular range of $\sim 10°$ 2θ (including both the Pb 111 and 200 diffraction peaks) for rapid data collection. An *in vacuo* ''standard,'' prepared by resolidifying a thick Pb film, provided a measure of the instrumental broadening ($\sim 0.15°$ 2θ full-width-at-half-maximum for the Pb 111 peak). For the surface melting studies, the x-ray divergence slit setting was wider than for the size-dependent melting measurements so that more intensity was obtained, particularly in the tails. The x-ray scans were taken for 1–20 min, depending on the temperature and the Pb 111 diffraction intensity.

III. ANALYSIS OF DIFFRACTION PEAKS

The integrated x-ray-diffraction intensity is proportional to the total volume of crystallites that are oriented to diffract. The diffraction peak shape reflects the average size and size distribution of the crystallites, with smaller crystallites producing broader diffraction peaks. Strain within the crystallites can also cause diffraction peak broadening and asymmetry. X rays scattered from liquid Pb add a very broad peak to the background under the Pb 111 diffraction peak.

In this study, Fourier analysis of the x-ray diffraction peak shapes provided the average crystallite size, size distribution, and strain.[44,45] The raw data was prepared first by subtracting the background due to the substrate and a variable quantity of liquid, and then by correcting the data for variations in the polarization, atomic form factor, Debye-Waller factor, and crystallographic structure factor. After a Fourier-series expansion about the diffraction peak's center-of-gravity, the Stokes correction was used to deconvolute instrumental broadening.[54] The final Fourier cosine and sine coefficients (A_L and B_L, respectively, at harmonic distance L) were normalized so that $A_0 = 1$. Uncertainties due to counting statis-

tics were propagated throughout the analysis (and given in parentheses).[55]

At each temperature, A_L is due to the crystallite size and strain distributions within the diffracting volume, i.e.,[44,45]

$$A_L = A_L^{Size} A_L^{Strain}, \qquad (3a)$$

where

$$A_L^{Strain} \approx 1 - 2\pi^2 (1/d_{hkl})^2 L^2 \langle \varepsilon_L^2 \rangle. \qquad (3b)$$

Here, d_{hkl} is the interplanar spacing of the reflection, hkl. $\langle \varepsilon_L^2 \rangle$ is the mean-squared strain or strain variance averaged over a diffracting column of length L.

The area-averaged crystallite size ($\langle L \rangle$) is obtained by extrapolating the initial Fourier coefficients to the abscissa, using a least-squares fit to Eq. (4) for improved accuracy:[44,45]

$$\langle L \rangle = -A_0/(dA_L/dL)_{L \to 0}. \qquad (4)$$

$\langle L \rangle$ is also known as the average column length. The Fourier shape function $A_L(D)$ for spherical crystallites of a single diameter is[56,57]

$$A_L(D) = 1 - 1.5(L/D) + 0.5(L/D)^3 \quad \text{for } L \leqslant D,$$

$$A_L(D) = 0 \quad \text{for } L > D, \qquad (5)$$

and $B_L(D) = 0$. It follows from Eqs. (4) and (5) that $\langle L \rangle = (2/3)\langle D \rangle$ for a sharp crystallite size distribution about average diameter $\langle D \rangle$. If the crystallites are distributed in size as volume fraction $\Gamma(D)$, then the aggregate Fourier coefficients are

$$A_L = \sum_D \Gamma(D) A_L(D), \quad \text{where} \sum_D \Gamma(D) = 1. \qquad (6)$$

Using Eq. (6), the crystallite size distribution can be determined by a least-squares fit of $\Gamma(D)$ to the measured Fourier coefficients A_L.

Defects in the crystallites may systematically reduce the measured crystallite size $\langle L \rangle$ from the true one $\langle L_t \rangle$, as follows:[44,45]

$$\langle L \rangle^{-1} = \langle L_t \rangle^{-1} + \langle L_d \rangle^{-1}, \qquad (7)$$

where $\langle L_d \rangle$ is the apparent size that is due to the defects including strain, deformation faults, and twins. Since $\langle L \rangle$ ranges from 8 to 16 nm here, it can be shown for the Pb 111 peak that the sum of these systematic uncertainties gives a maximum possible reduction in $\langle L \rangle$ from $\langle L_t \rangle$ of 6.5–13 %, respectively, (Appendix A).[47] These systematic uncertainties will be included separately from the statistical uncertainty.

IV. RESULTS

A. Sample morphology and cleanliness

Auger electron spectroscopy measurements confirmed that the freshly prepared Pb surface remained clean for tens of hours under the present vacuum conditions. Figures 1(a) and 1(b) are scanning electron micrographs of a typical sample. The micrographs were obtained *ex situ* following the size-dependent melting study, several additional melt-solidification cycles, and several hours at $T \geqslant 0.9$ in ultrahigh
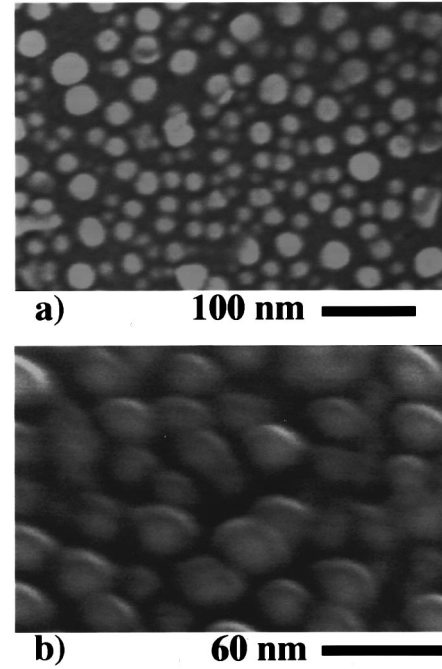

FIG. 1. Scanning electron micrographs at (a) 0° tilt and (b) 45° tilt of a typical Pb thin film deposited on Si.

vacuum. In Fig. 1(a), the view is along the surface normal. The gray background is the substrate. The white circles are Pb islands, which range in diameter between 5 and 35 nm and are separated by less than one diameter. In Fig. 1(b), the view is at 45° to the surface normal to accentuate the nearly spherical particle shape. Knowing the shape is roughly spherical, Eq. (5) can be used for the Fourier shape function of the crystallites.

B. Particle reorientation during melting

After sample preparation, x-ray measurements were obtained at $T = 0.730$, 0.870, 0.913, 0.926, 0.940, 0.950, 0.954, 0.958, 0.962, 0.965, 0.966, 0.967, and 0.968 of the bulk melting temperature. Figure 2 shows the scans obtained at $T = 0.730$, 0.954, and 0.965. The most striking observation is the intensity increase of the Pb 111 peak when T increases from 0.730 to 0.954, followed by a rapid intensity decrease at higher temperature.
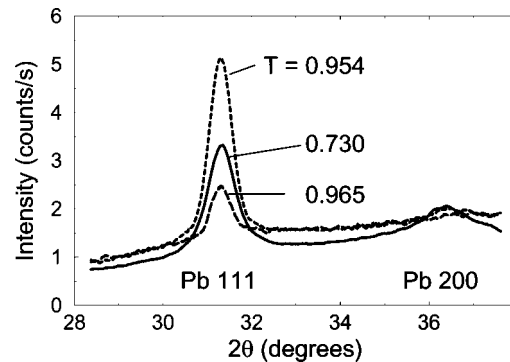

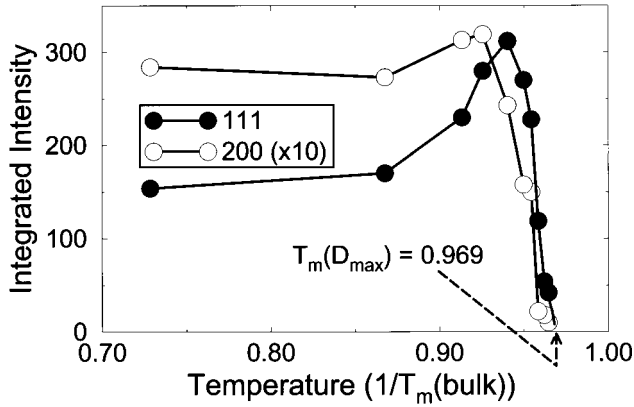FIG. 2. X-ray-diffraction scans of Pb 111 and 200 peaks at $T = 0.730$, 0.954, 0.965.

FIG. 3. Pb 111 and 200 diffraction intensity (background sub-tracted) versus temperature.

FIG. 4. Pb 111 diffraction peak shape and Fourier coefficients at low and high temperatures. *Inset:* Pb 111 diffraction peak shapes for lead particles at $T=0.730$ and 0.965 and for a Pb standard at room temperature. *Main:* filled circles indicate A_L at $T=0.730$; filled squares indicate B_L at $T=0.730$ showing negligible strain or faulting-induced assymetry; filled triangles indicate A_L at $T=0.965$ shows crystallite size distribution is altered by size-dependent melting; dashed line indicates $A_L(D)$ for 23 nm spherical crystallites and shows size distribution sharpens on approaching $T_m(D_{max})$; open circles indicate A_L after resolidifying the sample. $\langle L \rangle$ indicates the area-averaged crystallite size from the initial cosine coefficients at both temperatures.

Figure 3 shows these intensity changes more clearly. The increasing intensity can only be due to crystallites rotating and reorienting themselves into a preferred orientation with their (111) face parallel to the substrate and perpendicular to the diffraction vector. This kind of crystallite reorientation on an amorphous substrate has been seen before in the classic ''rotating sphere studies'' of interfacial phenomena.[18,58–61] The intensity variation is sensitive to the temperature, the heating rate (time scale≈1 min), and the choice of diffraction peak. Additional measurements indicate that the crystallites remain oriented upon cooling. Since both melting and crystallite rotation strongly modify the diffraction intensity, it must be concluded that the diffraction intensity by itself is an unreliable indicator of size-dependent melting.

Since the (111) orientation is preferred, the disappearance of all Pb 111 diffraction intensity occurs at the melting temperature of the last—and largest—crystallites in the sample,[18] which we designate to have diameter D_{max}. By extrapolating to zero intensity in Fig. 3, we find the melting temperature of these largest particles, $T_m(D_{max})$, to be 0.969. This is the only information on melting that we can obtain from the intensity data. Instead, we will now focus on the diffraction peak shape and its relation to the melting. All but the final three Pb 111 measurements had sufficient intensity for peak-shape analysis (i.e., filled circles in Fig. 3).

C. Size-dependent melting

Figure 4 compares the Pb 111 peak shapes and Fourier coefficients at $T=0.730$ and 0.965, slightly below $T_m(D_{max})$. The Pb 111 peak narrows with increasing temperature. Note, in particular, the disappearance of the strong tails at $T=0.965$. This is due to melting of the smaller crystallites. Next, we analyze the peak shapes via the Stokes-corrected Fourier coefficients.

The initial Fourier cosine coefficients at $T=0.730$ (filled circles) and 0.965 (filled triangles) yield an average crystallite size $\langle L \rangle$ equal to 7.9 (2) and 15.5 (11) nm, respectively [Eq. (4)]. According to Eq. (2) and since $T=0.965$ is only 0.004 below $T_m(D_{max})$, the crystallite size distribution should be quite narrow. Indeed, applying Eq. (5) to the data
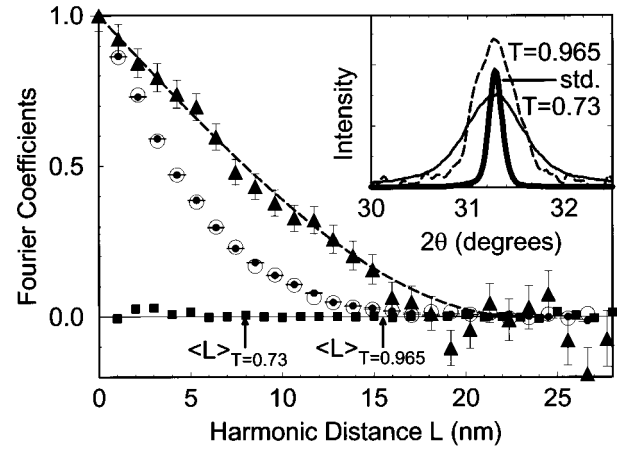
for $T=0.965$ (Fig. 4, dashed line) gives a good fit with a single size, $D_{0.965}=23$ (1) nm≈$(3/2)\langle L \rangle$ (as discussed earlier).

After the entire sample melted, at $T_m(D_{max})$, and cooled back to $T=0.730$, the Fourier coefficients were measured again (open circles in Fig. 4). Their similarity to A_L at $T=0.730$ before melting shows that the original crystallite size distribution is recovered after melting and resolidifying the entire sample. Consequently, the differences between the low- and high-temperature measurements are *not* due to crystallite growth via coarsening or coalescence.

The observed doubling of the average crystallite size must be due the crystallite size distribution shifting to a larger size at $T=0.965$ as the smaller particles have melted. To determine the crystallite size distribution, we fit Eq. (6) to the Fourier coefficients obtained at each temperature and thereby determined the volume fraction for four crystallite size bins (diameters of 6, 12, 18, and 24 nm). Figure 5 shows clearly the shifting of the crystallite size distribution to a larger size as one approaches $T=0.965$.

The area-averaged crystallite size increases monotonically with temperature, beginning around $T=0.9$ (Fig. 6). Fitting Eq. (2) (melting temperature versus crystallite size) to the data provides both a calibration for the bulk melting temperature and the measured value of α (dashed curve). The slope of $T_m(\langle D \rangle)$ versus $1/\langle D \rangle$ is -0.87 (6) nm (where $\langle D \rangle=1.5\langle L \rangle$) for $T \geq 0.94$. Within the statistical uncertainty of the experiment, the slope is unchanged after increasing $\langle L \rangle$ to remove the possible systematic effects of strain, microtwinning, and deformation faults that were evaluated earlier. Since $\langle L \rangle$ measures the average and not the smallest crystallite size present at each temperature, the measured slope overstates the value of α. A proper correction gives
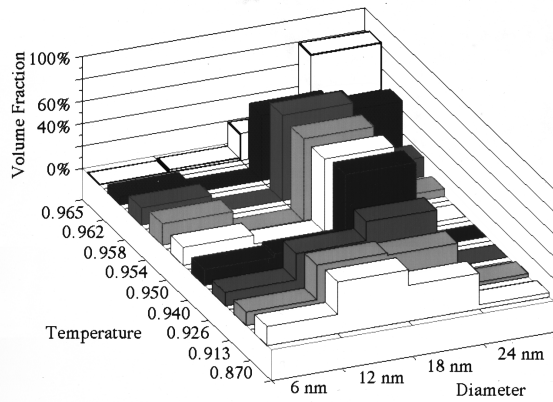
FIG. 5. Evolution of crystallite size distribution as temperature increases from 0.87 (front) to 0.965 (rear). Data are volume fractions (6–24 nm diameter) with the total volume normalized to unity.

FIG. 7. Pb 111 x-ray-diffraction peaks taken during two undercooling cycles (inset).

−0.62 (4) nm for the slope of $T_m(D)$ versus $1/D$ (see Appendix B). Substituting the corrected slope into Eq. (2) (0.62 nm $=4\alpha/\rho_s H$ using the bulk values of 11.3 g/cm^3 for ρ_s and 23.1 J/g for H), we have $\alpha=0.040$ (3) J/m^2 with the uncertainty derived from the original counting statistics. Using $T_m(D_{max})$, one also finds that $D_{max}=27$ nm, which is similar in size to the largest particles in Fig. 1.

The results show clearly that small particles melt at reduced temperatures, following Eq. (2). However, it remains to be shown whether a liquid skin envelops the crystallites as the size-dependent melting temperature is approached. If a liquid skin progressively consumes a crystallite, then the crystallite diameter would be reduced, and this could broaden the diffraction peak. However, in a polydispersed sample, if the liquid-skin growth is a weak function of temperature, then the peak broadening due to surface melting might be obscured by the peak narrowing resulting from the melting of smaller particles, as we observed in Fig. 6.

D. Small-particle surface melting

To determine if a liquid skin exists on crystallites, we performed x-ray-diffraction studies on a different sample
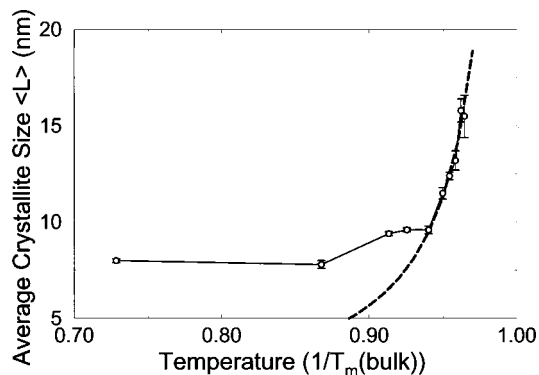

FIG. 6. Area-averaged crystallite size $\langle L \rangle$ versus temperature. A linear fit (dashed line) to data obtained at the six highest temperatures (for which the crystallite size distribution is expected to be sharp) provides the measured coefficient α for Eq. (2).
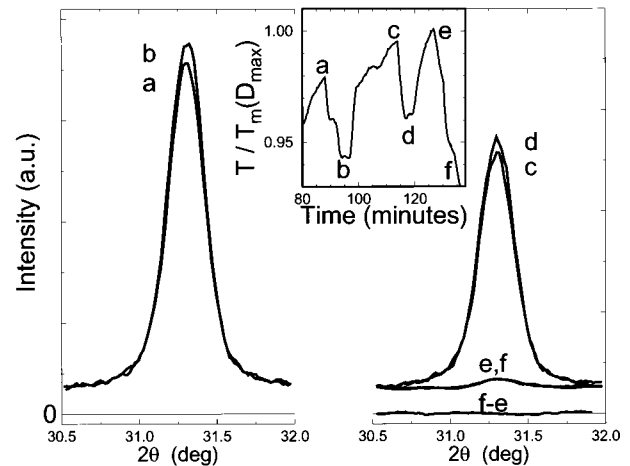
during ''undercooling'' cycles. The sample was first heated to near $T_m(D_{max})$ to melt most particles and promote liquid-skin formation on the remaining crystallites. Upon slight cooling, the liquid particles do not solidify (we were able to undercool by as much as 120 K) whereas the thickness of the liquid skin on the crystallites is expected to decrease reversibly.[10] Thus, undercooling provides a means of separating the effects of the surface melting from the size-dependent melting. X-ray-diffraction can measure the changing crystallite volume during an undercooling cycle, as we have shown in a preliminary report.[25]

Before the temperature excursion experiment, the sample was annealed for three hours above 90% $T_m(D_{max})$. The annealing increased the population of large, (111)-oriented crystallites available to diffract, and also minimized the spurious effects of coarsening and particle rotation during subsequent measurements. In Fig. 7, the Pb 111 x-ray-diffraction profiles, (a)–(f), were obtained at temperatures of 98.0, 94.3, 99.55, 96.0, 100.05, and 93.5 % $T_m(D_{max})$, respectively (inset). The 111 diffraction peak grew on cooling from (a) to (b) and from (c) to (d). Measurement (e) was taken at 100.05% $T_m(D_{max})$, showing melting of all Pb particles. Measurement (f) was obtained upon cooling to 93.5% $T_m(D_{max})$. The data from the latter two measurements are indistinguishable as the particles remain melted during undercooling. This proves that solidification of the liquid particles is negligible between 100% and 93.5% $T_m(D_{max})$. These results were reproduced with another sample.

During the temperature excursion between 98.0 and 94.3% $T_m(D_{max})$, the area-averaged crystallite diameter was 46 (2) nm with no apparent variation with the temperature. Upon further heating to 99.55% $T_m(D_{max})$, the intensity decreased 35% and the average crystallite diameter increased due to size-dependent melting. The diameter then remained constant at 52 (2) nm during the temperature excursion between 99.55 and 96 % $T_m(D_{max})$. If a liquid skin of uniform thickness τ envelops a crystallite at high temperature, then the crystallite diameter would change as follows:

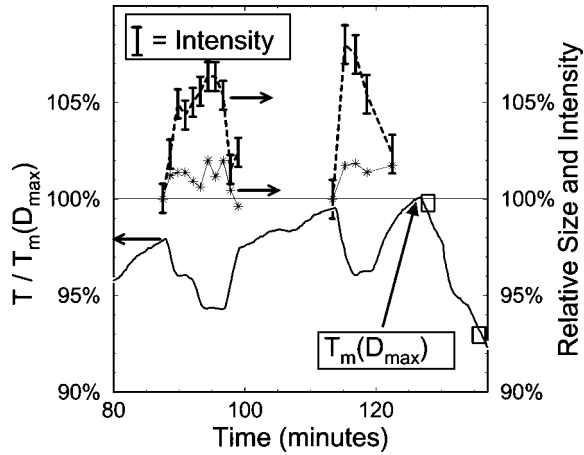$$\frac{\Delta(\langle D \rangle)}{\langle D \rangle} = -2\frac{\Delta\tau}{\langle D \rangle}. \quad (8)$$

FIG. 8. Temperature (bold line), diffraction intensity (I), and average crystallite size (asterisks) versus time for two undercooling cycles. Less than 1% intensity change can be attributed to the Debye-Waller effect. The remainder is due to surface melting and ~0.5 nm reversible liquid skin growth. The variation in the average crystallite size (~1.5%) is less than the statistical uncertainty at each point (~3%).

Therefore, Eq. (8) establishes an upper limit of 1.0 nm for the change in liquid-skin thickness for the two undercooling cycles beginning at 98 and 99.55 % $T_m(D_{max})$. [Note that when the uncorrected Fourier series at each temperature was normalized by the first series, then a marginally significant variation (~1.5%) was observed between the crystallite size and the temperature (asterisks in Fig. 8, which is discussed next).]

Figure 8 shows the variation of temperature and normalized diffraction intensity versus time. The intensity increases reversibly by 6 (1)% on cooling from 98 to 94.3 % $T_m(D_{max})$ with $\langle D \rangle = 46$ (2) nm. In the next temperature cycle, the intensity increases reversibly by 7(2)% on cooling from 99.55 to 96 % $T_m(D_{max})$ with $\langle D \rangle = 52$ (2) nm. The intensity change cannot be due to particle rotation or coalescence because it is reversible and immediate and because the sample had been annealed for three hours above 90% $T_m(D_{max})$. Also, simple calculations based on the Debye-Waller factor for the Pb 111 diffraction peak show that only a 1% intensity increase is expected for the 3.5% temperature reduction, including bulk and surface atomic vibrations.[62]

The remaining intensity change can be related geometrically to the growth of a uniformly thick liquid skin, as follows:

$$\frac{\Delta I}{I} = -6 \frac{\Delta \tau}{\langle D \rangle}. \tag{9}$$

Thus, $\Delta \tau = 0.38$ (8) and 0.52 (17) nm for the undercooling cycles beginning at 98.0 and 99.55 % $T_m(D_{max})$, respectively. Comparing the two undercooling cycles, the liquid skin growth is slightly greater at the higher temperatures, beginning at 99.55% $T_m(D_{max})$. Also, within the undercooling cycle that begins at 98.0% $T_m(D_{max})$, three fourths of the intensity increase occurs on cooling to 96.1% $T_m(D_{max})$, while only one fourth occurs on further cooling to 94.3% $T_m(D_{max})$. Thus, it appears that the liquid-skin growth in-

creases on approaching $T_m(D_{max})$, which is similar to flat-surface melting, e.g., of the Pb(110) surface.[10]

V. DISCUSSION

The three main results of this paper are

(A) X-ray-diffraction methods can reveal the size-dependent melting and the surface melting of nanocrystals;

(B) A measurement of the size-dependent melting temperature of Pb gave $T_m(D) = 1 - 0.62$ nm$/D$, i.e., Eq. (2) with $\alpha = 0.040$ (3) J/m^2; and

(C) Surface melting was observed, with ~0.5 nm liquid-skin growth just below the size-dependent melting temperature of 50 nm Pb crystallites.

The demonstration of liquid-skin growth gives unambiguous support to the liquid-skin melting model over the homogeneous melting model. The liquid nucleation and growth model remains possible because transient liquid-skin formation can occur even though the liquid-skin thickness and the melting temperature are indeterminate in this model. However, the liquid nucleation and growth model requires a more precise statement of the melting temperature or liquid skin thickness in order to be evaluated clearly (see below).

A. The x-ray-diffraction method

Our experimental approach, based on x-ray diffraction, has important advantages over prior methods in that quantitative measures of the particle size and state (i.e., crystallinity) are obtained by a single measurement with minimal spurious effects. Analysing the diffraction peak shape instead of the diffraction intensity is different from the approach taken in previous studies of size-dependent melting.

We also find that the crystallite reorientation and surface melting both occur in the same temperature range (cf. Figs. 3 and 8) and may be related to each other. Balluffi and Maurer[63] suggested that crystallite-substrate interfacial melting would cause the crystallite to rotate into low-γ_{sl} orientations, predominantly (111) and to a lesser extent (100), as we observed. It follows that the Pb-silica interface might have melted below the size-dependent melting temperature. In the present study of Pb nanocrystals, growth of the Pb(111)-silica interface might drive the (111) reorientation of the crystallites. While our results do not resolve the long-standing question of interfacial melting, the overlapping temperature for surface melting and crystallite reorientation is interesting.

It should be noted that the observed diffraction peak broadening is *not* due to multiply twinned structures (MTPs, i.e., icosahedra, decahedra, etc.) or quasimelting (i.e., rapid fluctuations among several particle structures and orientations)[34] for the following reasons. First, the present observation of slow Pb crystallite rotation (time scale ≈ 1 min) and slow coarsening (1 h) is much slower than the rapid quasimelting (1 s) observed previously by electron microscopy at room temperature.[24,34,64] Secondly, the above analysis and Appendix A reveal that the influence of strain broadening and microtwinning (hence the MTP population) is negligible in the present study. Finally, the observed narrowing and broadening of the diffraction peak occurs in conjunction with the melting and solidification of the Pb nano-

particles. Although some recent studies have observed MTP's and the quasimelting of encapsulated Pb nanoparticles by electron microscopy,[24,64] this might be caused by the encapsulating layer.[65–67] Also, Marks[34] has observed that "at least for lead particles, it is clear that there is more taking place due to the electron beam than can be simply accounted for by any type of electron-beam heating."

B. Size-dependent melting

The size-dependent melting temperature of Pb, $T_m(D) = 1 - 0.62(4)$ mm/D, has been measured here by using x-ray-diffraction under ultrahigh vacuum conditions.

Historically, tests of the theoretical melting models against experimental results on $T_m(D)$ have always been impeded by the commonality of Eq. (2) to all three models, as well as the uncertainty of the interfacial energies, especially $\gamma_{s\ell}$. Recent improvements in the determination of $\gamma_{s\ell}$ bring more meaning to the comparison.[28] For Pb: $\gamma_{sv} = 0.560(4)$ J/m^2 (Ref. 68) with $\pm 3\%$ variation,[27] $\gamma_{\ell v} = 0.452$ J/m^2,[68] and $\gamma_{s\ell} = 0.046$ J/m^2.[28]

Theoretically, the complete expressions for α in the melting models are (without the prior simplifications):

$$\alpha_1 = \gamma_{sv} - \gamma_{\ell v}(\rho_s/\rho_l)^{2/3} = 0.097 \text{ J/m}^2, \qquad (9a)$$

$$\alpha_2 = \gamma_{s\ell} - \gamma_{\ell v}\frac{(\rho_s/\rho_1) - 1}{1 + (2\tau/D)} = 0.031 \text{ J/m}^2, \qquad (9b)$$

$$0.046 \text{ J/m}^2 = \gamma_{s\ell} \leqslant \alpha_3 \leqslant 1.5[\gamma_{sv} - \gamma_{\ell v}(\rho_s/\rho_\ell)^{2/3}]$$
$$= 0.145 \text{ J/m}^2, \qquad (9c)$$

using $\rho_s/\rho_l = 1.035$ for Pb,[2] and taking $\tau/D \approx 0.01$ from the surface melting measurements.

When comparing the theories to the measured value of $\alpha[0.040(3)$ J/m$^2]$, the liquid-skin melting model (2) is clearly more satisfying than either the homogeneous melting model (1) or the liquid nucleation and growth model (3).

[The remaining discrepancy between α and α_2 could be removed as follows. Pluis *et al.*[11,12] note that the bulk interfacial energies (above) do not satisfy the relation $\Delta\gamma \approx 0$ that is needed to explain the variation in liquid-skin thickness with $\Delta\gamma$ on different flat-surface orientations $\{hkl\}$ of Pb. Instead, Pluis *et al.*[11,12] obtain a best fit with $\gamma_{\ell v} = 0.501$ J/m^2, $\gamma_{sv} = 0.561$ J/m^2 (having $\pm 3\%$ variation with $\{hkl\}$), and $\gamma_{s\ell} = 0.056$ J/m^2 (so that $\Delta\gamma \approx 0$). Using these values brings the liquid-skin melting model (i.e., $\alpha_2 = 0.039$ J/m^2) within the experimental uncertainty of the present measurement.]

C. Surface melting and liquid-skin growth

Our results show that the liquid skin on 50 nm Pb nanocrystals grows at roughly 0.1 nm per 1% temperature change near the melting temperature under clean conditions. The skin growth is two orders of magnitude smaller than what Lereah *et al.* reported using dark-field transmission electron microscopy on a 100 nm Pb particle constrained in a solid silica overlayer.[65–67] Bohr has shown that the overlayer could induce the observed temperature range of solid-liquid coexistence via pressurization effects during the melting.[66,67]

(The discrepancy could be resolved by repeating the electron microscopy measurements on unconstrained particles in ultrahigh vacuum.)

In order to compare the present liquid-skin growth near $T_m(D)$ to flat-surface melting near $T_m(\infty)$, two assumptions are necessary. First, we choose Pb(110) to be the "representative" flat-surface orientation of Pb because Stranski[5] posits that surface melting on (110) faces is intermediate between high-index and other low-index surface orientations, consistent with experimental observations.[10–12,26] Pb(110) has a liquid-skin thickness $\tau^{(110)} = \tau_0 \ln[\delta T_0/\delta T]$ with $\tau_0 = 0.3$ nm, $\delta T_0 = 164$ K, and δT is the temperature difference below the melting temperature.[10,12] Second, the temperature difference δT is taken as $\delta T = T_m(\infty) - T$ [i.e., instead of $T_m(D) - T$]. This interpretation of δT appears to be consistent with small-particle surface melting theories.[29,30,32]

With these two assumptions, one can readily compare our data $\Delta\tau$ on small-particle surface melting with the flat-surface melting $\Delta\tau^{(110)}$ over the same temperature excursion. It can be shown by using Eq. (2) that $T_m(D_{max}) = 0.992$ $T_m(\infty)$ for this sample. Beginning at 98.0% $T_m(D_{max})$, the first temperature excursion ($\Delta T = 0.037$ in Fig. 8) has given $\Delta\tau = 0.38(8)$ nm experimentally, while $\Delta\tau^{(110)} = 0.27$ nm on the flat Pb(110) surface over the same temperature excursion. Likewise, in the second temperature excursion beginning at 99.55% $T_m(D_{max})$, the measured $\Delta\tau = 0.52(17)$ nm is comparable to $\Delta\tau^{(110)} = 0.4$ nm. This comparison indicates that the measured liquid-skin growth on 50 nm crystallites is the same or slightly greater than $\Delta\tau^{(110)}$ for a flat Pb(110) surface over the same temperature excursion.

The Baker-Dash theory[29,30] of small-particle surface melting gives an enhanced liquid-skin thickness τ^{BD} on a nanocrystal compared to that on a representative flat surface at the same δT below the melting temperature; i.e., $\Delta\tau^{BD} = 0.35$ and 0.55 nm for the first and second temperature excursions, respectively (again assuming $\tau^{(110)}$ for the representative flat surface and δT the temperature difference). While our data then agree well with the Baker-Dash theory for this size and temperature range, the correction is within the experimental error. It is of course understood that the liquid skin may be nonuniform and that the above analysis yields only a value averaged over all crystallite surface orientations.

Finally, we find that an improved thermodynamic theory is needed to examine the melting and surface melting of nanocrystals, especially at temperatures close to $T_m(D)$. In the classical liquid-skin melting model, the liquid-skin thickness is a free parameter independent of size and temperature that has been fit empirically to experimental data at $T_m(D)$ in prior studies.[14,15,17,19,22,69] Models of small-particle surface melting, like the Baker-Dash theory, do not fully explain the final melting at the size-dependent melting temperature. As mentioned earlier, the liquid nucleation and growth model also deserves renewed attention.

VI. CONCLUSIONS

(1) The x-ray-diffraction peak shape clearly reveals the reduced melting temperature of the nanocrystals in agreement with theory.

(2) The diffraction intensity reveals crystallite reorientation near the melting temperature, which suggests that prior

results based solely on the diffraction intensity needed further confirmation.

(3) The reversible growth of a liquid skin has been demonstrated and is comparable to published data on flat-surface melting.

(4) Results giving the size-dependent melting temperature and the surface melting of small particles support the liquid-skin melting model over other models in the literature.

APPENDIX A: POSSIBLE EFFECT OF DEFECTS ON $\langle L \rangle$

The strain in copper filings[70] at 298 K gives $\langle L_d \rangle$ = 400 nm and reduces $\langle L \rangle$ less than 2% to 4% from $\langle L_t \rangle$, following Eq. (7).[44,45] Likewise, by taking the population of deformation faults to be equal to 0.003 (for copper filings at 298 K),[70] we have $\langle L_d \rangle \geq 250$ nm so that $\langle L \rangle$ is reduced by less than 3% to 6% from $\langle L_t \rangle$ in the present study. Finally, for the possible population of twin defects $\beta = 0.002(3)$, we have $\langle L_d \rangle \geq 520$ nm which gives less than 1.5% to 3% reduction in $\langle L_t \rangle$ (50% confidence), where β is computed from the measured shift of the 111 diffraction peak centroid relative to the peak maximum $[\Delta 2\theta = 0.007(8)°]$.[71] This also indicates that there is less than one twin per 520 nm on the four types of Pb{111} planes, which is much greater than the particle size and therefore is simply the limit of the analysis.

APPENDIX B: CORRECTION TO $T_m(\langle D \rangle)$

As a result of the size-dependent melting temperature, the crystallite size distribution has a lower limit $D_{\min}$, established by Eq. (2). As $D_{\min}$ increases with temperature, the area-averaged crystallite diameter $\langle D \rangle$ also increases but at a different rate. The variation of $\langle D \rangle$ with $D_{\min}$ can be expressed analytically. Equations (4)–(6) are used with the summations replaced by integrals. It is assumed simply that from $D_{\min}$ to $D_{\max}$ the crystallite size distribution $\Gamma(D)$ is sharp and decreases linearly to zero, as follows:

$$\Gamma(D) = c(D_{\max} - D), \tag{B1}$$

where c is a positive constant and $\Gamma(D)$ is the volume fraction. Using Eqs. (5), (6), and (B1), the Fourier coefficients for an array of spherical crystallites are

$$A_L = \int_{D_{\min}}^{D_{\max}} c(D_{\max} - D)\left[1 - 1.5\frac{L}{D} + 0.5\left(\frac{L}{D}\right)^3\right]dD. \tag{B2}$$

Solving for $A_0 = 1$ gives

$$c = 2(D_{\max} - D_{\min})^{-2}. \tag{B3}$$

It also follows from Eq. (B2) that

$$\left(\frac{\partial}{\partial L}A_L\right)_{L \to 0} = \int_{D_{\min}}^{D_{\max}} c(D_{\max} - D)\left[\frac{-1.5}{D}\right]dD, \tag{B4}$$

which is easily integrated. For a sharp crystallite size distribution, $\langle D \rangle = 1.5\langle L \rangle$, as discussed in the text. Since $D_{\max}$ is a constant, we can define $D_{\max} = 1$ so that $D_{\min}$ and $\langle D \rangle$ are fractions of $D_{\max}$. After substituting A_0, $\langle D \rangle$, and Eq. (B4) into Eq. (4), the area-averaged crystallite diameter is calculated to be

$$\langle D \rangle = (-0.5)(1 - D_{\min})^2[1 - D_{\min} + \ln(D_{\min})]^{-1}. \tag{B5}$$

A plot of $\langle D \rangle$ versus $D_{\min}$ from 0.5 to 1 is very nearly linear. The average slope (taken from the endpoints) is $\Delta\langle D \rangle / \Delta D_{\min} = 0.71$. Multiplying $\Delta\langle D \rangle / \Delta D_{\min}$ by the measured slope of $T_m(\langle D \rangle)$ (i.e., 0.87 nm) gives 0.62 nm for the corrected slope of $T_m(D)$ versus $1/D$, as is used in the text.

[1] J. W. Christian, *The Theory of Transformations in Metals and Alloys* (Pergamon, New York, 1975).

[2] A. R. Ubbelohde, *The Molten State of Matter* (Wiley, New York, 1978).

[3] J. G. Dash, Contemp. Phys. **30**, 89 (1989).

[4] M. Faraday, *Faraday's Diary* (Bell, London, 1933).

[5] I. N. Stranski, Naturwissenschaften **28**, 425 (1942).

[6] P. Z. Pawlow, Z. Phys. Chem. Abt. A **65**, 545 (1909).

[7] H. Reiss and I. B. Wilson, J. Colloid Sci. **3**, 551 (1948).

[8] P. R. Couchman and W. A. Jesser, Nature (London) **269**, 481 (1977).

[9] R. W. Cahn, Nature (London) **323**, 668 (1986).

[10] J. W. M. Frenken and J. F. van der Veen, Phys. Rev. Lett. **54**, 134 (1985).

[11] B. Pluis, A. W. D. van der Gon, J. W. M. Frenken, and J. F. van der Veen, Phys. Rev. Lett. **59**, 2678 (1987).

[12] B. Pluis, A. W. D. van der Gon, J. F. van der Veen, and A. J. Riemersma, Surf. Sci. **239**, 265 (1990).

[13] M. Takagi, J. Phys. Soc. Jpn. **9**, 359 (1954).

[14] P. A. Buffat and J. P. Borel, Phys. Rev. A **13**, 2287 (1976).

[15] P. A. Buffat, Ph.D thesis, Ecole Polytechnique Federale de Lausanne, 1976.

[16] G. L. Allen, R. A. Bayles, W. W. Giles, and W. A. Jesser, Thin Solid Films **144**, 297 (1986).

[17] R. P. Berman and A. E. Curzon, Can. J. Phys. **52**, 923 (1974).

[18] J. F. Pocza, A. Barna, and P. B. Barna, J. Vac. Sci. Technol. **6**, 472 (1969).

[19] C. J. Coombes, J. Phys. F **2**, 441 (1972).

[20] Y. I. Petrov, Fiz. Met. Metalloved. **19**, 219 (1965).

[21] V. P. Skripov, V. P. Koverda, and V. N. Skokov, Phys. Status Solidi A **66**, 109 (1981).

[22] C. R. M. Wronski, J. Appl. Phys. **18**, 1731 (1967).

[23] S. J. Peppiatt and J. R. Sambles, Proc. R. Soc. London, Ser. A **345**, 387 (1975).

[24] R. Kofman, P. Cheyssac, and R. Garrigos, Phase Transit. **24**, 283 (1990).

[25] K. F. Peters, Y.-W. Chung, and J. B. Cohen, Appl. Phys. Lett. **71**, 2391 (1997).

[26] J. C. Heyraud, J. J. Metois, and J. M. Bermond, J. Cryst. Growth **98**, 355 (1989).

[27] J. C. Heyraud and J. J. Metois, Surf. Sci. **128**, 334 (1983).

[28] N. Eustathopoulos, Int. Metall. Rev. **28**, 189 (1983).

[29] M. B. Baker and J. G. Dash, J. Cryst. Growth **97**, 770 (1989).

[30] J. W. Cahn, J. G. Dash, and H. Fu, J. Cryst. Growth **123**, 101 (1992).

[31] D. Beaglehole, J. Cryst. Growth **112**, 663 (1991).

[32] D. Nenow and A. Trayanov, J. Cryst. Growth **99**, 102 (1990).

[33] R. R. Vanfleet and J. M. Mochel, Surf. Sci. **341**, 40 (1995).

[34] L. D. Marks, Rep. Prog. Phys. **57**, 603 (1994).

[35] K. J. Hanszen, Z. Phys. **157**, 523 (1960).

[36] H. Reiss, P. Mirabel, and R. L. Whetten, J. Phys. Chem. **92**, 7241 (1988).

[37] M. J. Stowell, T. J. Law, and J. Smart, Proc. R. Soc. London, Ser. A **318**, 231 (1970).

[38] T. Castro, R. Reifenberger, E. Choi, and R. P. Andres, Phys. Rev. B **42**, 8548 (1990).

[39] S. L. Lai, J. Y. Guo, V. Petrova, G. Ramanath, and L. H. Allen, Phys. Rev. Lett. **77**, 99 (1996).

[40] A. N. Goldstein, C. M. Echer, and A. P. Alivisatos, Science **256**, 1425 (1992).

[41] M. Schmidt, R. Kusche, W. Kronmuller, B. von Issendorff, and H. Haberland, Phys. Rev. Lett. **79**, 99 (1997).

[42] W. Contrata, J. J. Mitchell, and J. M. Mochel, Ultramicroscopy **48**, 297 (1993).

[43] S. J. Peppiatt, Proc. R. Soc. London, Ser. A **345**, 401 (1975).

[44] L. H. Schwartz and J. B. Cohen, *Diffraction from Materials* (Springer-Verlag, New York, 1987).

[45] B. E. Warren, *X-ray diffraction* (Dover, New York, 1990).

[46] P. Zschack, J. B. Cohen, and Y.-W. Chung, J. Appl. Crystallogr. **21**, 466 (1988).

[47] K. F. Peters, Ph.D. thesis, Northwestern University, 1997.

[48] K. Christmann, Surf. Sci. Rep. **9**, 1 (1988).

[49] R. W. Joyner, K. Kishi, and M. W. Roberts, Proc. R. Soc. London, Ser. A **358**, 223 (1977).

[50] R. W. Hewitt and N. Winograd, Surf. Sci. **78**, 1 (1978).

[51] M. Hansen, *Constitution of Binary Alloys* (McGraw-Hill, New York, 1958).

[52] T. B. Massalski *et al.*, *Binary Alloy Phase Diagrams* (American Society for Metals, Metals Park, OH, 1986).

[53] R. E. Honig and D. A. Kramer, RCA Rev. **30**, 285 (1969).

[54] A. R. Stokes, Proc. Phys. Soc. London **A61**, 382 (1948).

[55] W. H. Schlosberg and J. B. Cohen, J. Appl. Crystallogr. **16**, 304 (1983).

[56] W. L. Smith, J. Appl. Crystallogr. **9**, 187 (1976).

[57] G. Porod, in *Small Angle X-ray Scattering*, edited by O. Glatter and O. Kratky (Academic, New York, 1982).

[58] G. Herrmann, H. Gleiter, and G. Baro, Acta Metall. **24**, 353 (1976).

[59] J. Shirokoff and U. Erb, Philos. Mag. Lett. **58**, 255 (1988).

[60] J. Shirokoff and U. Erb, Thin Solid Films **151**, 65 (1987).

[61] R. W. Cahn, Nature (London) **375**, 363 (1995).

[62] G. A. Somorjai, *Introduction to Surface Chemistry and Catalysis* (Wiley, New York, 1994).

[63] R. W. Balluffi and R. Maurer, Scr. Metall. **22**, 709 (1988).

[64] T. Ben-David, Y. Lereah, G. Deutscher, J. M. Penisson, A. Bourret, R. Kofman, and P. Cheyssac, Phys. Rev. Lett. **78**, 2585 (1997).

[65] Y. Lereah, G. Deutscher, P. Cheyssac, and R. Kofman, Europhys. Lett. **12**, 709 (1990).

[66] J. Bohr, Europhys. Lett. **14**, 85 (1991).

[67] Y. Lereah, G. Deutscher, P. Cheyssac, and R. Kofman, Europhys. Lett. **14**, 87 (1991).

[68] V. K. Kumikov and K. B. Khokonov, J. Appl. Phys. **54**, 1346 (1983).

[69] J. R. Sambles, Proc. R. Soc. London, Ser. A **324**, 339 (1971).

[70] D. E. Mikkola and J. B. Cohen, in *Local Atomic Arrangements Studied by X-ray Diffraction*, edited by J. B. Cohen and J. E. Hilliard (Gordon and Breach, New York, 1965), Vol. 36.

[71] J. B. Cohen and C. N. J. Wagner, J. Appl. Phys. **33**, 2073 (1962).